

Metal enriched gaseous halos around distant radio galaxies: Clues to feedback in galaxy formation ¹

Michiel Reuland^{1,2,3}, Wil van Breugel^{1,4}, Wim de Vries^{1,2}, Michael A. Dopita⁵, Arjun Dey⁶,
George Miley³, Huub Röttgering³, Bram Venemans³, S.A. Stanford^{1,2}, Mark Lacy⁷, Hy
Spinrad⁸, Steve Dawson⁸, Daniel Stern⁹ & Andrew Bunker¹⁰

wil@igpp.ucllnl.org

ABSTRACT

We present the results of an optical and near-IR spectroscopic study of giant nebular emission line halos associated with three $z > 3$ radio galaxies, 4C 41.17, 4C 60.07 and B2 0902+34. Previous deep narrow band Ly α imaging had revealed complex morphologies with sizes up to 100 kpc), possibly connected to outflows and AGN feedback from the central regions. The outer regions of these halos show quiet kinematics with typical velocity dispersions of a few hundred km s⁻¹, and velocity shears that can mostly be interpreted as being due to rotation. The inner regions show shocked cocoons of gas closely associated with the radio lobes. These display disturbed kinematics and have expansion velocities and/or velocity dispersions > 1000 km s⁻¹. The core region is chemically evolved, and we also find spectroscopic evidence for the ejection of enriched material in 4C 41.17 up to a distance of ≈ 60 kpc along the radio-axis. The dynamical structures traced in the Ly α line are, in most cases, closely echoed in the Carbon and Oxygen lines. This shows that the Ly α line is produced in a highly clumped medium of small filling factor, and can therefore be used as a tracer of the dynamics of HzRGs. We conclude that these HzRGs are undergoing a final jet-induced phase of star formation with ejection of most of their interstellar medium before becoming “red and dead” Elliptical galaxies.

Subject headings: galaxies: active — galaxies: formation — galaxies: high-redshift — galaxies: individual (B2 0902+34, 4C 60.07, 4C 41.17) — quasars: emission lines

1. Introduction

There is compelling evidence that in galaxies the formation and evolution of the central stellar bulge and the massive nuclear black hole are intimately related (Magorrian et al. 1998; Ferrarese & Merritt 2000; Gebhardt 2000). Understanding this coevolution of galaxy spheroids and their central massive black holes is one of the

¹Institute of Geophysics and Planetary Physics, Lawrence Livermore National Laboratory, L-413, Livermore, CA 94550 USA

²Physics Department, University of California at Davis, One Shields Avenue, Davis, CA 95616 USA

³Sterrewacht Leiden, Postbus 9513, 2300 RA Leiden The Netherlands

⁴University of California, Merced, P.O. Box 2039, Merced, CA 95344

⁵Research School of Astronomy and Astrophysics, The Australian National University, Cotter Road, Weston Creek, ACT2611, Australia

⁶NOAO, 950 N. Cherry Ave., Tucson, AZ 85719 USA

⁷SIRTF Science Center, Caltech, MS 220-6, 1200 E. California Boulevard, Pasadena, CA 91125 USA

⁸Department of Astronomy, University of California at Berkeley, Berkeley, CA 94720 USA

⁹Jet Propulsion Laboratory, California Institute of

Technology, Mail Stop 169-327, Pasadena, CA 91109 USA

¹⁰Institute of Astronomy, University of Cambridge, Madingley Road, Cambridge CB3 0HA UK

¹Based on observations at the W.M. Keck Observatory, which is operated as a scientific partnership among the University of California, the California Institute of Technology, and the National Aeronautics and Space Administration. The Observatory was made possible by the generous financial support of the W.M. Keck Foundation.

major outstanding issues in modern cosmology. Because they are readily located by their ultra-steep spectrum radio properties, the high redshift radio galaxies (HzRGs; $z > 3$) provide an efficient means to locate and study the environment and physics of newly-forming galaxies. There are at least two reasons why HzRGs are key in attempts to understand the physical processes involved. First, they rank among the most luminous, largest, and most massive galaxies known in the early Universe (e.g., De Breuck et al. 2002). Secondly, we observe them early in the epoch of galaxy formation at a time when their super-massive black holes (SMBHs) are highly active, and while their relativistic jets are interacting most strongly on their host galaxies.

Within the framework of the standard Λ Cold Dark Matter (Λ -CDM) scenario, it is believed that massive galaxies grow in a hierarchical fashion through the merging of smaller stellar and dark matter halo objects. Whether their central black holes grow in similar fashion or whether they are primordial objects (Loeb 1993; Silk & Rees 1998; Kauffmann & Haehnelt 2000), the energetic outflows and the ionizing radiation from these central active SMBHs are expected to profoundly influence the evolution both of their parent galaxies and of the surrounding environment. Recent models describing the formation of massive galaxies and clusters provide further evidence for the importance of this feedback (Benson et al. 2003; Springel, Di Matteo, & Hernquist 2005). Additionally, outflows could provide a source for the chemical enrichment of the intergalactic medium seen at high redshifts (e.g., Rauch, Sargent, & Barlow 2001; Aguirre et al. 2001). While there is consensus that feedback in some form must be important, there is an ongoing debate about which manifestations dominate and the scales on which they operate.

Because they are themselves massive galaxies in the early universe, HzRGs are located in the regions of large matter overdensities and within regions rich in forming galaxies. Indeed, many are known to be embedded in regions of dense interstellar medium (ISM) and in environments containing the earliest known galactic clusters (e.g., McCarthy 1993; van Ojik et al. 1996, 1997; Athreya et al. 1998; Pentericci et al. 2000; Papadopoulos et al. 2000). These gaseous reser-

voirs enable us to study in detail the feedback processes occurring at high redshift.

In an earlier paper (Reuland et al. 2003) we described the results from narrow-band imaging observations of unprecedented sensitivity of three HzRGs (B2 0902+34, 4C 60.07, and 4C 41.17). These images were obtained at the Keck II 10 m telescope using custom-made, high-throughput interference filters with bandpasses centered at the redshifted Ly α line. The observations revealed very luminous ($L_{\text{Ly}\alpha} \approx 10^{45}$ erg s $^{-1}$) and extended (≈ 200 kpc) emission line nebulae with spectacular features not previously seen, such as long filamentary structures, ionization cones, and multiple sharply bounded regions of enhanced emission, all indicative of strong interactions as expected from the scenario painted above. We argued that these extended Ly α nebulae might represent gas cooling in massive CDM halos, supplying new material for the continued growth of the galaxies at their center. This feeding could then be responsible for feedback mechanisms through radio jets, supernova explosions, and radiation pressure from the AGN, resulting in large scale outflows. The extended X-ray halo around 4C 41.17 provides further evidence for a highly interactive environment in such systems (Scharf et al. 2003).

However, with only morphological data, important issues concerning possible origins for the filaments and large-scale structures well beyond the radio sources could not be tackled. Because Ly α is a resonance line, it is also important to resolve the question of whether the nebulae represent truly extended ionized halos, or rather, are due to Ly α photons which are produced near the central AGN and are scattered off neutral hydrogen halos. Many other questions concerning the structure, origin, and fate of the emission-line gas remain. For example: is the gas organized in shells, filaments, or cloudlets? What is the source of ionization and what is the chemical composition of the gas? Can the outflows regulate the growth of galactic bulge and black-hole? Can they expel metals from the deep potential wells to enrich the intergalactic and inter-cluster medium?

In order to better understand the kinematics, abundances, and ionization mechanisms of these halos we obtained optical and near-infrared spectra with the Keck telescopes to measure the extent, intensity, and kinematics of Ly α and other

non-resonance lines, [He II], [O II] and [O III], at various position angles across the nebulae. This paper discusses the results of these spectroscopic observations.

The structure of the paper is as follows: The sample selection, observations and data analysis are described in §2. In §3 we present results for individual objects. §4 is a discussion of the observed kinematics and line ratios of the halos. The implications for the origin and fate of the emission line halos are discussed in §5 and our conclusions are given in §6.

Here we adopt the concordance cosmological parameters $\Omega_M = 0.27$, $\Omega_\Lambda = 0.73$ and $H_0 = 71 \text{ km s}^{-1} \text{ Mpc}^{-1}$. The age of the Universe is $1.7 - 1.9 h_{71}^{-1} \text{ Gyr}$ at the redshifts ($z = 3.4 - 3.8$) of our galaxies, and the angular-to-linear transformation is $\approx 7.4 h_{71}^{-1} \text{ kpc arcsec}^{-1}$.

2. Observations and data analysis

2.1. Sample Selection

The three objects selected for the spectroscopic follow-up observations are shown in Table 1 with their positions and adopted redshifts. They were selected from amongst the galaxies observed in the course of our Keck imaging program (Reuland et al. 2003). The reasons for their inclusion in the spectroscopic program are summarized as follows.

4C 41.17 at $z = 3.8$, was one of the first HzRGs to be discovered (Chambers, Miley & van Breugel 1990) and for many purposes serves as an archetype HzRG. Optical (Dey et al. 1997) as well as sub-mm wavelength observations (Dunlop et al. 1994; Ivison et al. 2000) have shown that it is a massive forming galaxy with a star formation rate of up to several thousand $M_\odot \text{ yr}^{-1}$. Recently, very extended X-ray emission was found around 4C 41.17, which follows the $\text{Ly}\alpha$ morphology closely (Scharf et al. 2003).

We selected 4C 60.07 ($z = 3.8$; Chambers et al. 1996; Röttgering et al. 1997) because it shows both spatially and kinematically resolved CO emission (Papadopoulos et al. 2000; Greve et al. 2005). Interestingly, in Reuland et al. (2003) it was found that the $\text{Ly}\alpha$ halo has a very extended ($76 h_{71}^{-1} \text{ kpc}$) filament which appears orthogonal to the major axis of the CO and dust emission.

B2 0902+34 ($z = 3.4$; Lilly 1988) was selected because it is thought to be a protogalaxy, dominated by young stars (Eisenhardt, & Dickinson 1992). So far, it is one of only a handful of HzRGs for which neutral hydrogen has been detected in absorption against the radio continuum (Uson, Bagri & Cornwell 1991; Cody & Braun 2003).

2.2. Optical and Near-Infrared Spectroscopy

Figure 1 shows the different slit positions used in the program overlaid on contour representations of the narrow-band $\text{Ly}\alpha$ images of the galaxies. In contrast to most previous spectroscopic studies of HzRGs, most of the slits were not placed directly along the radio axis. The specific instrumental setups are given in Table 2. The data reduction techniques are described below.

2.2.1. Optical Observations: LRIS

Most of the optical observations were carried out using the Low-Resolution Imaging Spectrometer (LRIS; Oke et al. 1995) at the Cassegrain focus on the 10 m Keck I Telescope. The data were collected with various instrumental setups using both the long-slit mode and multi-slit masks designed to obtain spectra for ≈ 15 targets in the field simultaneously (as part of a survey looking for associated galaxies in the proto-cluser; Croft et al. 2006 in preparation). The red-sensitive LRIS-R camera was employed. This uses a Tektronix 2048 \times 2048 CCD detector with a pixel scale of $0''.215 \text{ pixel}^{-1}$.

All of the spectroscopic reductions were performed using standard methods and the NOAO IRAF² package (Tody 1993). Skylines were used to improve the first order wavelength calibration based on arc spectra to better than 0.3 \AA rms . The instrumental resolution was measured from the unblended skylines. Flux calibrations were performed using observations of standard stars such as Feige 110 and Feige 34 (Massey et al. 1988). The extended emission of 4C 41.17 filled the narrow slits of the multi-object spectroscopic program, rendering accurate sky subtraction difficult.

²IRAF is distributed by the National Optical Astronomy Observatory, which is operated by the Association of Universities for Research in Astronomy, Inc., under cooperative agreement with the National Science Foundation.

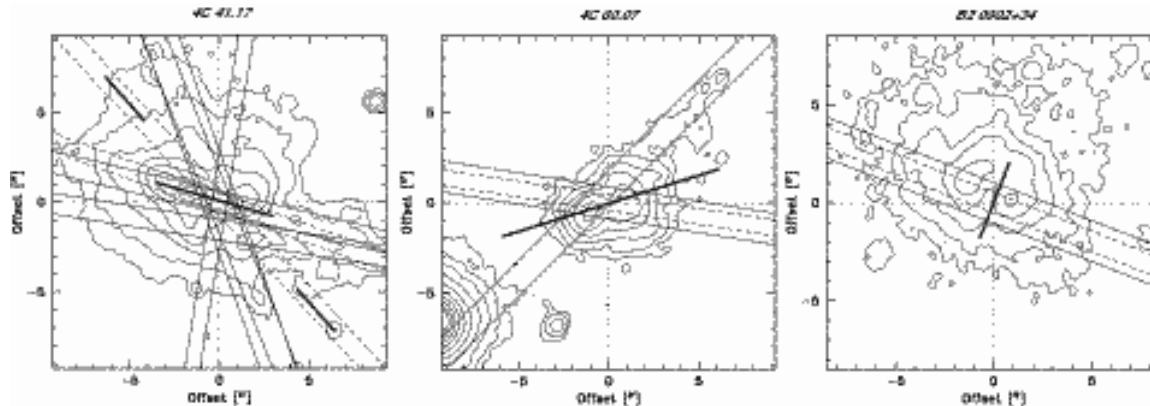


Fig. 1.— Contour representations of the Ly α emission line halos around 4C 41.17, 4C 60.07, and B2 0902+34 (left, middle, right) with the various PAs at which they were studied overlaid. In this figure, north is at the top and east at the left. The solid and dashed lines correspond with slit positions of the optical and near-IR spectroscopy respectively and the dotted lines indicate the positions of the radio cores. The bold lines represent the direction of the radio axes. In the case of 4C 41.17 two axes are shown, corresponding to the inner and outer radio lobes. For each object the contours indicate observed surface brightnesses of $6.7 \times 10^{-19} \times (6, 12, 25, 50, 100, 200, 400, 800)$ erg s $^{-1}$ cm $^{-2}$ arcsec $^{-2}$; see Reuland et al. (2003).

This does not seriously affect the kinematics and relative fluxes of interest for this paper.

2.2.2. Optical Observations: ESI

One set of observations along the filament of 4C 60.07 was made during the night of UT 2001 February 25, using the Echelle Spectrograph and Imager (ESI; Sheinis et al. 2000) at the Cassegrain focus of the Keck II 10 m telescope in low-dispersion mode. The detector used is a high-resistivity MIT-Lincoln Labs 2048×4096 CCD with a plate scale of $0''.154$ pixel $^{-1}$. Exposures were broken into integrations of 1800 seconds each, one of which had to be halved because of time constraints. We performed $6''$ offsets between each integration. The data were rotated over an angle depending on the position of the object on the slit, to align the dispersion axes. The wavelength calibration varies slightly with slit position, hence we shifted the spectra along the dispersion axes. This first order approximation is sufficiently accurate for the region of interest $4300\text{\AA} - 9200\text{\AA}$ (corresponding to approximately $900\text{\AA} - 1920\text{\AA}$ in the rest frame). Subsequent data reduction was done using standard methods in IRAF.

2.2.3. Near-IR Spectroscopy: NIRSPEC

The near-infrared spectra were obtained using the 10 m Keck II Telescope with its Near-Infrared Spectrograph (NIRSPEC; McLean et al. 1998). The slit dimensions were $0.76'' \times 42''$ slits giving low-resolution ($R \approx 1400 - 1900$) spectra in wavelength ranges chosen to include the H β , [O II] and [O III] lines of the target galaxies (see Table 2 for details). In this low-resolution mode, the 1024×1024 ALADDIN InSb detector has a plate scale of $0''.143$ pixel $^{-1}$. We obtained sets of 900 s integrations each with $\approx 5 - 10''$ spatial offsets between exposures.

The NIRSPEC spectra need to be corrected for the spectral curvature and spatial distortions caused by the high-throughput optics. A general correction would require rectification onto a slit position-wavelength grid based on a wavelength solution from skylines and coadded exposures of a standard star. However, since no continuum is apparent in our spectra, we have only extracted small regions lying close to the emission lines. This approach requires only a simple rotation over an angle which depends on the wavelength of interest to provide a local calibration of the wavelength along the slit.

The data were flat-fielded and corrected for cos-

mic rays and bad pixels in the standard fashion. In order to remove the strong near-IR skylines, and a sky frame scaled to the brightness of unsaturated sky lines near the emission line of interest was subtracted. Subsequently, the frames were cropped, rotated, and coadded. Flux calibration was done with standard stars of spectral type A0V, B3, and G4, and was consistent to within 10%.

2.3. Data analysis

For the data analysis the spectra were registered in position with radio maps from the literature (Carilli, Owen & Harris 1994; Carilli 1995; Carilli et al. 1997). The zero points of the spatial scales correspond with the radio core. This was achieved by identifying the core with the centroid of the continuum emission. If no continuum emission was visible, we identify the core with either the spatial region that shows the broadest line emission, or by bootstrapping to spectra for which the core could be reliably identified. These results were then checked with the narrow-band images, correlating with the peaks and dips in the observed intensity. This resulted in a total uncertainty less than $0.5''$ in the relative spatial offsets.

The velocity scale used in the analysis is relative to the systemic velocity derived from the He II $\lambda 1640$ line (the adopted systemic redshifts are given in Table 1). The kinematic information was obtained from the 2-D spectra using a program written in IDL making use of the publicly available fitting routine MPFIT³. The data were coadded within apertures matched to the seeing in order to increase the signal-to-noise ratio and ensure that the extracted spectra are not correlated. We then determined the velocity centroid, FWHM (corrected for instrumental broadening measured from unsaturated skylines, and assuming that the widths add in quadrature). The peak and baseline fluxes were determined by fitting a single Gaussian and baseline to each trace. Single Gaussians provide a good fit to the outer regions and in order to allow a direct comparison with the central regions similarly, we have chosen to treat all regions consistently using the simpler approach. The single Gaussian decomposition for high surface brightness emission may break down when these regions are embedded in more

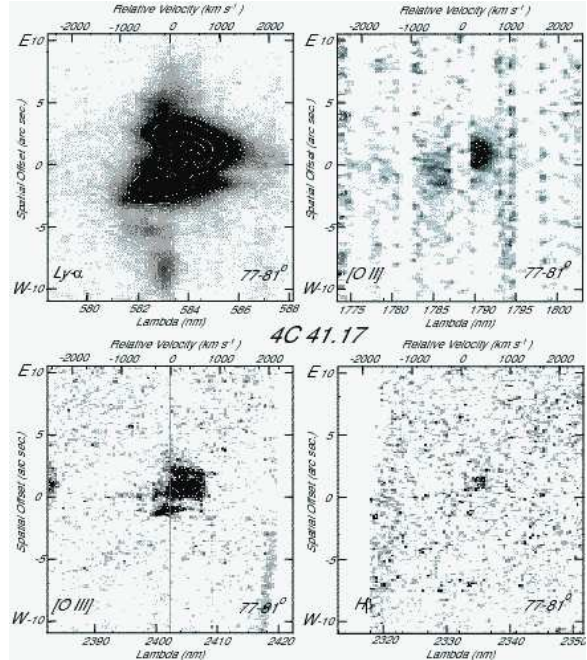


Fig. 2.— Grayscale representations of the 2-D spectra of 4C 41.17 centered at the Ly α , [O II] $\lambda 3727$, H β , and [O III] $\lambda 5007$ lines. The velocities are indicated relative to the systemic redshift determined from the He II line. The zero points of the spatial scales correspond with the position of the radio core as identified with the broad line and continuum emission. Note that the peaks of the line emission corresponding with the position of radio knot B2 in Carilli, Owen & Harris (1994) are $1''$ E of the nucleus. It can be seen (most easily in the [O III] $\lambda 5007$ spectrum) that there are $0.5''$ offsets between the broad lines and the central depression. The [O II] spectrum is rich in very strong skylines. These have been masked off to better show the structure of the [O II] line emission.

smoothly varying large scale low surface brightness envelopes.

3. Dynamical Results

Figures 2, 5, and 9 show 2-D optical and near-IR spectra of 4C 41.17, 4C 60.07, and B2 0902+34 centered at the emission lines most relevant to our discussion. It is immediately obvious, that many of the lines are very broad, and show strong spatial variation both in their velocity centroids and their

³Available at <http://cow.physics.wisc.edu/~craig/idl/fitting.html>

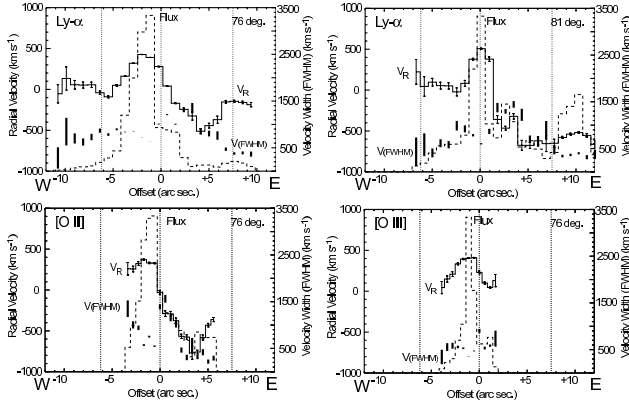


Fig. 3.— Relative velocities (solid lines), velocity dispersion (bars), and normalized surface brightness profiles (dashed lines) as determined from spectra with slit positions parallel to the radio axis for the Ly α , [O II], and [O III] emission lines of 4C 41.17. Top to bottom: Ly α along PA=76°, Ly α for PA=81°, [O II] for PA=70°, and [O III] for PA=68°. The spatial zeropoints correspond with the position of the radio core and the dotted lines represent the position of the radio lobes projected on the slit. East is at the right in all of these panels. The bar and symbol size indicate the 1σ uncertainties on the measurements. Note that the fits to the [O II] emission are affected by the strong skylines and that the slit along PA=81° did not go through the radio core.

FWHMs. In some cases continuum emission was also detected, but only from the central regions, within 3'' of the nucleus. Since the main interest of this paper is the extended emission, here we will focus our discussion on the nebular lines.

For both 4C 41.17 and 4C 60.07 the oxygen line profiles closely resemble the bright inner parts of the Ly α emission. Since self-absorption cannot be important in the strong forbidden lines, this suggests that the Ly α line is giving useful information about the kinematic structure despite being subject to resonance scattering. This can only be possible if the interstellar gas is highly clumped. If this is true in the inner regions, it is probably also true in the outer regions. In any case, even if the line is being resonantly scattered in the outer regions, it would likely still provide a fair (although possibly velocity biased) measure of the neutral gas kinematics.

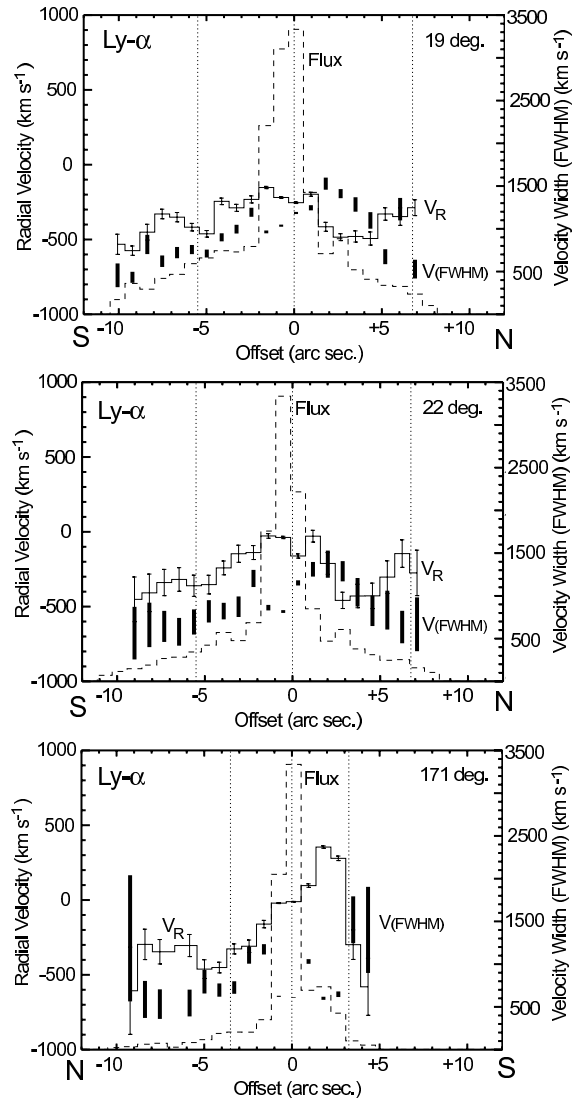


Fig. 4.— Similar to Fig. 3 but for the Ly α emission along the slits that lie more or less perpendicular to the radio axis of 4C 41.17. PA=19° (top), PA=22° (middle), and PA=171° (bottom).

Figures 3, 4, 6, and 10, summarize radial velocities, FWHMs, and the run of relative surface brightness of the halos as a function of distance from the radio core for different position angles. These figures show clear evidence for a distinction between disturbed and more quiescent regions. The inner regions have higher surface brightnesses, are characterized by large velocity dispersions ($\text{FWHM} \approx 1500 \text{ km s}^{-1}$), and seem

to be embedded in low surface brightness regions with FWHMs of order $\approx 500 \text{ km s}^{-1}$. In §4 we will discuss the general implications of these diagrams. First, we describe the individual sources.

3.1. Notes on individual objects

3.1.1. 4C 41.17: General Remarks

Dey et al. (1997) have discussed the brightest part ($2'' \times 1''$) of the extracted 1-D optical spectrum of 4C 41.17 at PA = 76° in detail. They determined a redshift $z = 3.79786 \pm 0.00024$ based on the He II line. Furthermore they found evidence for stellar absorption lines, and low polarization indicating that a young stellar population contributes significantly to the rest-frame UV continuum emission.

The 2-D spectra along the radio axis (PA 76° plotted in fig. 3) show that the Ly α , [O II], and [O III] emission line regions are very extended (over approximately $20''$, $10''$, and $6''$, respectively). The Ly α and [O III] lines both show two separate components straddling the radio core with peak fluxes separated by about $3''$. Careful inspection reveals that these components are present also in the [O II] line, with the red part of the western component missing due to a skyline near $\lambda = 17880 \text{ \AA}$. The dip in between the emission peaks is expected since the narrow-band Ly α and radio image overlays showed the core to be highly obscured (see Reuland et al. (2003)).

The large extent of the nebula in the [O II], and [O III] emission lines shows immediately that the whole Ly α halo is enriched in heavy elements. This immediately discounts the possibility that the emission line halo represents in-falling pristine gas. This point will be discussed further below.

A second item of note is that the velocity gradient in the halo and the velocity dispersions observed in the lines are comparable. This shows that the halo is a highly turbulent and disordered structure.

The image overlays indicated that the position of the radio core is offset by $0.5''$ to the NE from the central dip in the emission. In the spectra, the position of the radio core is revealed by a narrow high velocity tail on the [O III] profile, extending out to -1500 km s^{-1} and clearly visible in figure 2. In the Ly α profile, the nucleus is marked by a faint tail extending out to over $+2000 \text{ km s}^{-1}$ the

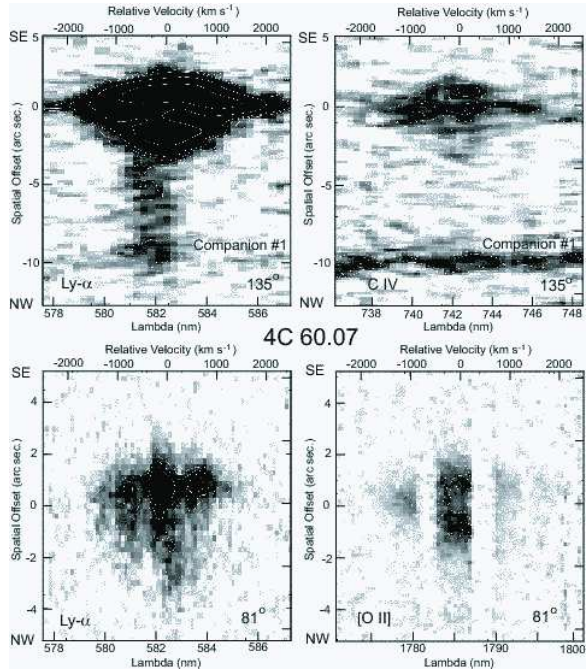


Fig. 5.— Similar to fig. 2. Grayscale representations of the 2-D spectra of emission line halo around 4C 60.07. The top left and top right panel respectively show Ly α and C IV emission along the filament with PA = 135° . The bottom left and right panel show Ly α and [O II] $\lambda 3727$ along the radio axis with PA = 81° .

negative velocity tail presumably being obscured by resonant scattering.

3.1.2. 4C 41.17: Kinematics

Dey et al. (1997) discerned the presence of both narrow and broad components in the central regions of the Ly α and [O III] emission lines of 4C 41.17 with FWHMs of $\approx 500\text{-}600 \text{ km s}^{-1}$ and $\approx 1200\text{-}1300 \text{ km s}^{-1}$ respectively. Figure 3 shows that these high velocity dispersions extend along the radio axis to the outer radio lobes. Beyond the limit of the radio lobes there is a break in velocity, the kinematics become more quiescent, and the velocity centroids change from being blue-shifted (-500 to -700 km s^{-1} along the Western lobe) to near systemic. Perpendicular to the radio axis (see Fig. 4) the kinematics follow a smooth gradient and the broad emission lines are found only in the central region of $\approx 3''$ ($\approx 20 \text{ kpc}$) wide, identified by its sharp peak in peak surface brightness.

This bright emission is associated with the inner radio lobes, and has been successfully ascribed to radiative shocks at the boundary of the expanding cocoon (Bicknell et al. 2000).

Except for the high velocity tail originating close to the AGN and discussed above, the Oxygen lines show narrower line components than the Ly α line, with FWHMs $\approx 600 \text{ km s}^{-1}$. The measured velocities and velocity dispersions likely reflect the true motions of the gas, whereas Ly α is additionally broadened by resonant scattering into the damping wings. The measurements on the [O III] line are likely to be much more reliable than the [O II] line because the line is brighter, is less reddened, and is not so badly cut about by night sky lines. Furthermore, corrections to the FWHM do not need to be made (in contradistinction to the [O II] doublet), and finally, it can be observed closer to the nuclear region than [O II], because of its higher critical density (see e.g., di Serego Alighieri et al. 1997).

Two very important results are found from the near-IR spectroscopy. First, as has been noted in the previous section, despite the obvious resonant broadening, the velocity structure of Ly α closely resembles that of [O III]. Secondly, there is [O II] emission in the velocity regime -200 to -1000 km s^{-1} extending from the nucleus to $7-8''$ west of the nucleus, whereas the [O III] emission appears to be much more centrally concentrated. We will discuss this further in §4.1.

The Ly α emission appears to show a strong velocity shear in its kinematically quiescent outer parts as yet undisturbed by the expansion of the radio source along the radio axis. By contrast, the kinematic profiles obtained with slit positions perpendicular to the radio axis (see fig. 4) show a fairly symmetric velocity distribution. This is indicative of an overall shear or rotation of the $\approx 200 \text{ kpc}$ diameter Ly α halo about its major axis.

The velocity structure of the bulk of the emission line gas appears predominantly red-shifted in the Oxygen, H β , and Ly α lines. A similar red-shift is seen in the extended CO J=4–3 emission (De Breuck et al. 2005), suggesting that the AGN may be offset from the systemic redshift of the galaxy. The central CO component is situated at a relative velocity of -125 km s^{-1} . The location of this CO component coincides in spatial position and velocity with the Ly α gap be-

tween the “cloud” and the galaxy as discussed in Reuland et al. (2003), suggesting that the dense molecular gas is absorbing the Ly α emission at this location.

3.1.3. 4C 60.07: General Remarks

The ESI spectrum of 4C 60.07 (PA = 135° ; fig. 5) shows a clear trace of continuum emission over approximately $3''$ which we associate with the position of the radio core and the unobscured optical nucleus. Comparison of this identification with the extent of the Ly α filament extending towards to N-W narrow-band image (Fig. 1) and which is visible in the lower part in the spectrum, shows that the nucleus has been located to within $0.5''$. Based on the He II line at $7855.7 \pm 1.1 \text{ \AA}$ we infer a redshift $z = 3.7887 \pm 0.0007$, in agreement with Röttgering et al. (1997).

3.1.4. 4C 60.07: Kinematics

The 2-D Ly α emission line (Fig. 6) shows interesting structure: crescent shaped clouds surround a gap at the position of the radio core near the systemic velocity of the galaxy. The spatial structure was expected from the narrow-band image, but the kinematic substructure is unusual. A comparable lack of Ly α emission near the systemic velocity of the galaxy has been found in a Ly α galaxy associated with the SSA-22 protocluster (Wilman et al. 2005) and the large Ly α halo recently discovered by the *Spitzer Space Telescope* (Dey et al. 2005). It seems reasonable to attribute these velocity profiles to complex radiative transport effects of the resonantly scattered Ly α emission in dense (dusty) media (e.g., Neufeld 1990; Ahn 2004) since these sources are strong submillimeter (rest-frame far-IR) emitters (Papadopoulos et al. 2000; Chapman et al. 2001). However, the similarity of the profiles of the Ly α line and the C IV line in this region suggest, rather, an interaction of the radio lobe with a cocoon of material.

The morphologies of the Ly α and [O II] spectra at PA = 81° (fig 5) are remarkably similar, providing further justification for the use of Ly α as a useful tracer of the dynamics of these systems, despite the problems of resonance scattering. Both lines have very high velocity FWHMs of $\approx 100 \text{ \AA}$ or $\approx 1600 - 1700 \text{ km s}^{-1}$, rather large for HzRGs. They are however smaller than for the

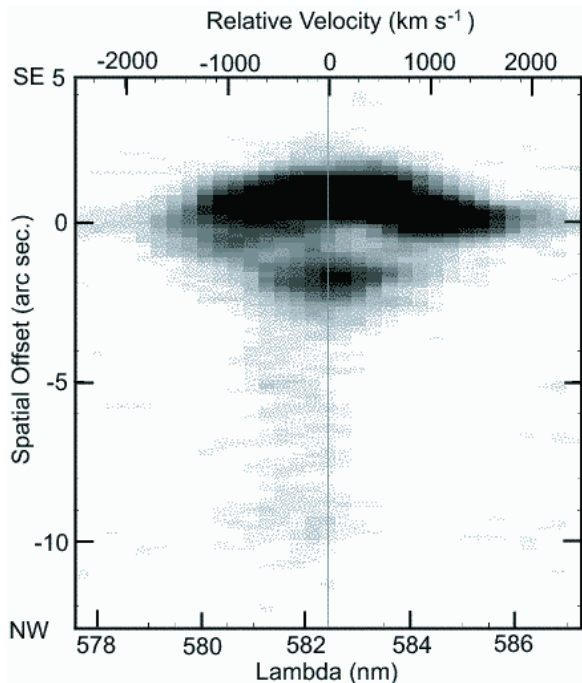


Fig. 6.— An expanded grayscale representation of the 2-D spectrum of 4C 60.07 centered at the redshifted Ly α line showing the filament and the crescent shaped arcs surrounding a depression in the emission that is identified with the location of the both radio core and unobscured optical nucleus. This kinematical signature is probably the result of a shock interaction between the radio lobe and its cocoon.

spectrum at PA = 135° which shows a FWHM of $\approx 2600 \text{ km s}^{-1}$. All of this is suggestive of the strong radiative shocks produced in an interaction of a powerful radio source with a surrounding dense interstellar medium.

The emission line profile across the Ly α gap can be fit with two Gaussian components with central wavelengths of $5839.9 \pm 0.5 \text{ \AA}$ and $5806.8 \pm 0.4 \text{ \AA}$ and FWHMs of $12.8 \pm 0.5 \text{ \AA}$ and $10.6 \pm 0.3 \text{ \AA}$ respectively. However, it is probably better to fit the whole bright region to a single expanding shell by a velocity ellipsoid, estimated by fitting an ellipse to the position : velocity curve obtained for the two peaks in line intensity at each spatial position. The fit obtained depends somewhat on both the position angle of the observation and on the line which is used to measure it, but all are consistent

with an expansion velocity of $1100 \pm 200 \text{ km s}^{-1}$.

3.1.5. 4C 60.07: The Ly α Filament

Perhaps the most striking feature of the emission line nebula surrounding 4C 60.07 is the extended Ly α filament. Imaging showed this to be of fairly constant surface brightness, sharply bounded on the NE side, and much more “fluffy” and rather ill-defined on the SW side close to the main emission region. The tip of the filament is cospatial with a small galaxy suggesting a causal connection. In Figure 8 we present the spectrum of this filament obtained with the ESI instrument.

Figures 6 and 7 show that the filament is offset from the systemic velocity of the radio source by approximately -200 km s^{-1} . The central wavelength fit by a single Gaussian yields $\lambda \approx 5818.1 \pm 0.3 \text{ \AA}$ or -175 km s^{-1} relative to the systemic velocity at $z = 3.789$. The line has a FWHM of $20 \pm 1 \text{ \AA}$ corresponding to a (deconvolved) velocity dispersion of $\approx 300 \text{ km s}^{-1}$. The fact that there is no evidence for a strong ($> 100 \text{ km s}^{-1}$) velocity gradient across the filament seems to indicate that it must be moving in the plane of sky.

Observations with mm-interferometers of the redshifted CO J=4–3 transition in 4C 60.07 have found two kinematically and spatially separate gaseous reservoirs (Papadopoulos et al. 2000). Recently this has been confirmed by VLA observations of the CO J=1–0 transition (Greve et al. 2005). An overlay of the Ly α image with the mm-observations, *see* fig. 5 in Reuland et al. (2003), suggests that the filament extends in a direction perpendicular to the major axis of the molecular gas, reminiscent of the (polar ejection) morphology of a galactic superwind. The CO J=4–3 observations showed a gas-rich narrow component with a FWHM of $\approx 150 \text{ km s}^{-1}$ at a velocity of -224 km s^{-1} to the galaxy. This same component has now been independently detected by its CO J=1–0 emission at a relative velocity of $-220 \pm 40 \text{ km s}^{-1}$ with a FWHM of 165 km s^{-1} .

As is the case for 4C 41.17, the optical spectroscopic observations show similar velocities for the molecular and emission line gas. This corroborates the idea of a superwind, as it provides a dynamical connection between the filament and the gas fueling the nuclear AGN. If this is the case, the source of the ionization may be either shocks or

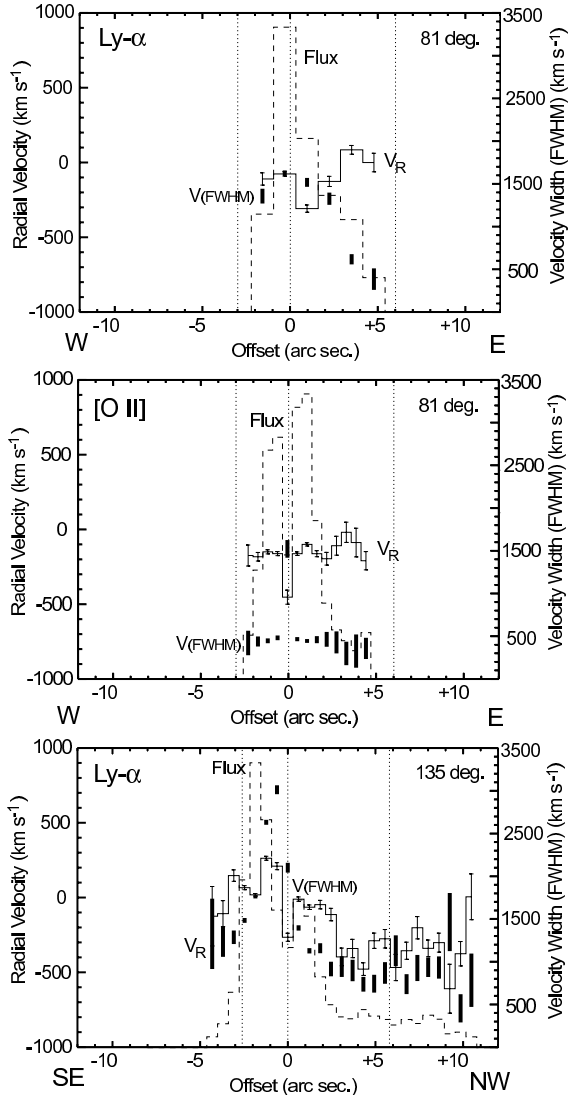


Fig. 7.— Similar to fig. 3 but for 4C 60.07. Ly α (top) and [O II] (middle) emission along PA=81 $^\circ$ and Ly α emission along PA=135 $^\circ$ (bottom).

photoionization from the central nucleus.

The superwind interpretation of the Ly $-\alpha$ filament does however present certain difficulties. In particular, it is hard to understand how this feature, over 70 kpc in length, manages to remain so well-collimated and kinematically quiescent over such a distance if it were related to a high-speed outflow (albeit in the plane of the sky). However, the filter cut-off may play an important role here, since the the observed velocity of the filament is

very close to the filter cut off. Thus, it may give the appearance of a sharp boundary, but may not be one in actuality. Possibly a slit placed over “empty sky” next to the filament would reveal other portions of the filament at different velocities. As alternative possibility may be that it represents an accretion filament or a tidally stripped gas stream extending from the active galaxy. In this case, the both the quiescence of its velocity field, and the similarity of the systemic velocities of the filament and of the molecular reservoir would both find a more natural explanation. Photoionization by the central AGN would then be the most probable cause of the ionization of the filament. On balance, this accretion or tidal stripping scenario seems to provide the most convincing explanation for the filament.

The galaxy at the tip of the filament is most likely to be a chance superposition. Figure 8 shows the 2-D and 1-D spectra of this galaxy (Companion # 1), and a second companion galaxy (Companion #2) which also fell on the slit. The spectrum of Companion #1 is very similar to, but fainter than Companion #2. The brighter galaxy shows an emission feature, identified as the [O II] line and a break near 7000 \AA , while the overall shape of the spectrum for the fainter galaxy is similar but without an evident break. Identifying the line at 7047.0 \AA with redshifted [O II] λ 3727 yields a redshift of $z = 0.891$ for the galaxy. This implies that it is a foreground object and not causally connected to the filament, despite its suggestive location.

3.1.6. B2 0902+34: General Remarks

The optical spectrum obtained for B2 0902+34 is more sensitive than previous observations reported in the literature (Lilly 1988; Martin-Mirones et al. 1995). We have detected Ly α emission over an extent of $\approx 10''$ with a complex multi-component spatial and velocity structure (cf. fig 9) and have detected extended (3'') continuum emission from the core over the entire wavelength range with an almost constant surface brightness. The Ly α profile shows galaxy-wide blue-shifted absorption by neutral hydrogen.

As is evident from Table 3 and Figure 9, the inferred redshifts depend on both the emission line and the position of the aperture used. Much of this is due to the absorption optical depth effects

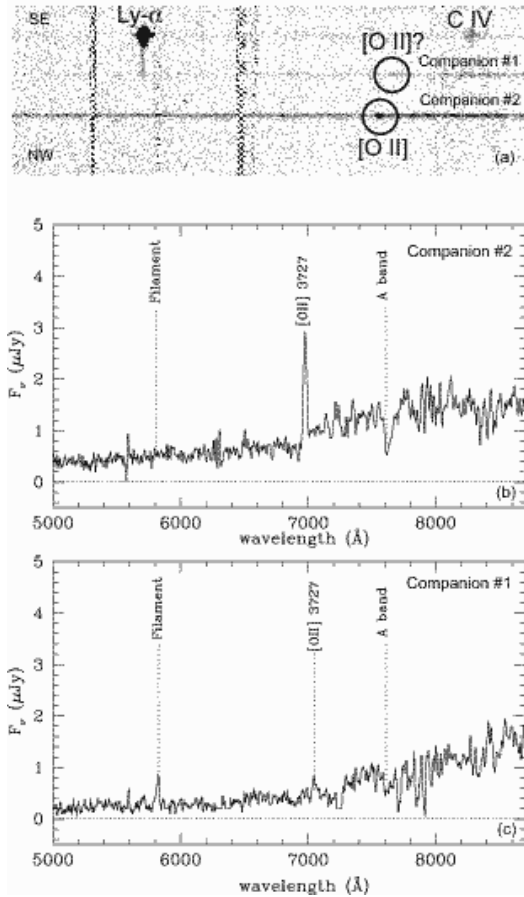


Fig. 8.— (a) A 2-D spectrum of the galaxy (# 1) at the tip of the Ly α filament of 4C 60.07, together with the spectrum of a brighter companion galaxy (# 2) which happened to lie on the slit. The position of the galaxy might suggest a physical association with the Ly α filament of 4C 60.07. However, the spectrum of companion galaxy #1 bears close resemblance to the brighter foreground galaxy #2 shown in panels (b) and (c), respectively. The circles in panel (a) indicate emission lines which are probably redshifted [O II] λ 3727 in both foreground galaxies, identified in the spectra of panels (b) and (c).

in the line. The He II line at $7199.35 \pm 0.5 \text{ \AA}$, extracted in a $2''$ wide aperture centered at the radio core, is probably most representative of the systemic velocity of the galaxy. From this we infer a redshift $z = 3.3886 \pm 0.0003$. This is slightly less than that reported previously by Lilly (1988) and Martin-Mirones et al. (1995). They inferred

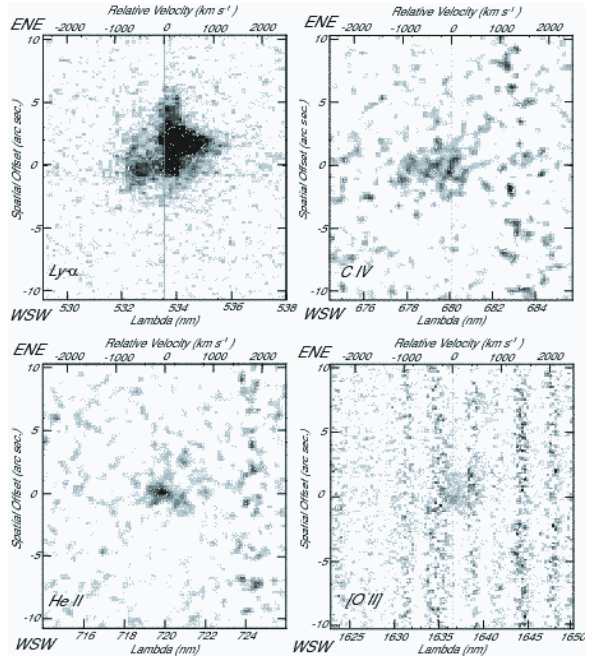


Fig. 9.— Similar to fig. 2, but for B2 0902+34. The top left panel shows the line emission profile for Ly α , top right C IV, bottom left He II, and bottom right [O II].

$z = 3.395$ and $z = 3.391$ respectively. However, these reported redshifts are entirely consistent with redshift estimates we derive using other lines in the same aperture, emphasizing the difficulty of assigning single redshifts to such complex and self-absorbed systems.

3.1.7. B2 0902+34: Kinematics

The He II line is only a few hundred km s^{-1} wide and may be slightly extended, with its position of maximum surface brightness centered at the position of the radio nucleus. We can therefore argue that it arises from photo-ionization of the dense gas surrounding the nucleus. The [O II] line is broad and spatially extended, but is too faint to allow a detailed comparison with the kinematics of the other lines.

Given that B2 0902+34 shows associated H I absorption against the radio continuum it is important to see whether this is present also in the Ly α profile. This emission line shows a self-absorption feature on the blue side of the profile centered at $\lambda = 5331.58$ ($z = 3.3857$), and which

can be fitted with a Voigt profile with a column density of $1.8 \times 10^{14} \text{ cm}^{-2}$ and Doppler parameter $b = 195 \pm 11 \text{ km s}^{-1}$. The inferred blue shift is $\approx 100 \text{ km s}^{-1}$. This cannot be the same gas that causes H I absorption against the radio continuum, since Briggs, Sorar, & Taramopoulos (1993) and Cody & Braun (2003) infer a redshift $z_{\text{abs}} = 3.3962$ with $N_{\text{H}} = 3 \times 10^{21} \text{ cm}^{-2}$ and $\text{FWHM} = 120 \text{ km s}^{-1}$ for the absorbing gas. It is probable that the dense gas giving the H I absorption lies close to the nucleus, and any absorption that this may have produced in the Ly α line is completely veiled by the frequency re-distribution produced by multiple scattering events.

The Ly α absorption can possibly be identified with a galaxy-wide outflow of material. In this respect, it is very similar to the galaxy-wide outflow identified by Wilman et al. (2005) in a Ly α galaxy associated with the SSA-22 protocluster. We will return to this point in the discussion.

The underlying Ly α emission profile revealed by fig. 9 is very interesting, as it shows evidence of a strong velocity shear amounting to nearly 1000 km s^{-1} across the central arc sec. The upper (NE) component has the typical triangular shape resulting from spatially extended absorption that is blue-shifted relative to the systemic velocity (cf. Dey 1999), and it is terminated by the self-absorption on the blue side. The lower (SW) component may well have an underlying shape which is the symmetrically reversed version of the NE component, but the self-absorption makes this difficult to trace, and the line reaches its maximum brightness at a relative velocity of -500 km s^{-1} , as it emerges from under the absorption. Because of the self absorption, a gaussian fit to the line profile is not valid, and yields spuriously large values, as can be seen in fig. 10.

The C IV $\lambda 1549$ emission is both spatially extended and broad ($\approx 1000 \text{ km s}^{-1}$) and is centered on the nucleus. The line broadening in the nucleus is probably, once again, the result of a direct interaction between the relativistic outflow associated with the peculiar radio source (see Carilli 1995, for details) and its dense cocoon of interstellar medium.

4. Discussion

4.1. Emission Line Diagnostics

The relative intensities of emission lines are, in principle, powerful diagnostic tools for studying the excitation mechanisms, metallicities and physical conditions in the emission line gas associated with AGN. Diagnostic diagrams for optical line ratios have been most extensively used to probe the gas in nearby active galaxies, where evidence for both jet- and accretion- powered shocks and for photoionization by the central AGN has been adduced (e.g., Bicknell, Dopita & O’Dea 1997; Dopita et al. 1997; Groves, Dopita & Sutherland 2004a,b). Consequently these relationships have been best calibrated for rest-frame optical lines. However, line diagnostic diagrams applicable to both shock- and photo-ionized AGN have been developed for use in the UV (Allen, Dopita & Tsvetanov 1998; Groves, Dopita & Sutherland 2004b).

Until recently, for most HzRGs (De Breuck et al. 2000) or for the 3C radio galaxies (Best, Röttgering, & Longair 2000a,b; Inskip et al. 2002a,b) only the rest-frame UV lines have been available. The optical line diagnostics have previously not been commonly used because of calibration difficulties and the limited sensitivity of near-IR spectrographs on telescopes of the 2-4 m class.

We would like to be able to use both UV and optical emission line diagnostics to determine the mechanism that is responsible for ionizing these extended emission line nebulae. The most likely candidates are: photoionization by radiation from an AGN or stars, shock heating, and shocks with precursors that photoionize the region ahead of the shock by radiation from the gas. Studies of $z \approx 1$ radio galaxies have shown that the dominant ionization mechanism may depend on the evolutionary state of the radio source (e.g., Best, Röttgering & Longair 2000a,b; Inskip et al. 2002a,b). Generally, it was found that the emission line gas of small (i.e. young) sources is shock ionized, but as the radio source expands beyond the host galaxy, interactions with the gas decrease and photoionization by the AGN takes over. As De Breuck et al. (2000) noted, for HzRGs the situation may be more complex.

Before we investigate these line diagnostics, we shall first use global energy requirements to con-

strain important source parameters on the basis of both photoionization and shock models. The total Ly α fluxes of the extended emission line regions are of order 10^{-14} ergs $^{-1}$ cm $^{-2}$, yielding luminosities $L_{\text{Ly}\alpha} \approx 10^{45}$ ergs $^{-1}$ (Reuland et al. (2003)). If the source of ionization is an active nucleus, then the luminosity of the source derives either from the UV photons which it produces, or from the mechanical energy of the jets which it powers. These luminosities can be derived from the theoretical ratio of the Ly $-\alpha$ flux to the total flux in both shock and photoionization models. To do this we use the shock models from Dopita & Sutherland (1996), and assume that the PdV work implied by this luminosity is the mechanical energy flux of the jet. For the justification of this assumption, see Bicknell, Dopita & O’Dea (1997). For photoionization, we use the radiation-pressure dominated photoionization models from Groves, Dopita, & Sutherland (2004a,b), assuming a power-law spectrum with index $\alpha = -1.4$ ($f_\nu \approx \nu^\alpha$). From these we derive either an ionizing radiative or a mechanical energy flux of at least 1.1×10^{46} ergs $^{-1}$. This flux is consistent with a typical luminous embedded QSO.

Alternatively, some of the ionization may be due to young stars such as are found in the numerous clumpy components of the Southern region of 4C 41.17 (van Breugel et al. 1999), and whose formation has probably been triggered in the dense cocoon surrounding the central radio jet (Dey et al. 1997; Bicknell et al. 2000). In this case, assuming a stellar radiation field with an effective temperature of 42,000K, we infer (using the Kennicutt (1998) calibration) that a star formation rate of at least $3000 M_\odot \text{yr}^{-1}$ would be needed to ionize the halo. This star formation rate is remarkably close to what is inferred from rest-frame far-IR observations (Dunlop et al. 1994; Stevens et al. 2003). However, this does not necessarily imply that stellar photoionization is the dominant ionization mechanism. Photoionization by stars usually results in Ly α equivalent widths less than 240 \AA (assuming stellar populations at solar metallicity; Charlot & Fall 1993) and would seem inconsistent with the large equivalent widths observed ($\approx 500 \text{ \AA}$; Dey et al. 1997). The strength of the C IV lines and other high-excitation species also militates against a purely stellar origin of the ionizing flux. Indeed,

Bicknell et al. (2000) have used the emission spectrum to infer that shocks are the dominant source of ionization in this region, and have used the flux to determine the PdV work being done by the relativistic jet. However, away from the radio axis photoionization by stars may well become more important. 4C 41.17 is a young system and recent modeling suggests that any primordial stellar populations could be very efficient in emitting significant amounts of ionizing flux while remaining virtually undetectable in the optical (c.f., Fosbury et al. 2003; Panagia et al. 2003).

Using the observed line ratios, better constraints on the ionizing process can be derived. Dey et al. (1997) determined the following ratios for the narrow rest-frame UV lines of 4C 41.17: C III]/C IV ≈ 0.14 (≈ 0.7 for total fluxes) and C IV/He II ≈ 2.4 . The latter is close to the maximum of 3.1 predicted by photoionization models. Although the narrow emission line strengths of C III], C IV, and He II can be matched by a simple nuclear AGN photoionization model with solar metallicity clouds, a high ionization parameter $U \lesssim 0.1$, and a power-law ionizing source with index $\alpha = -1.5$, Dey et al. (1997) and Bicknell et al. (2000) argue that the dominating ionizing mechanism is shocks rather than photoionization the nucleus.

Figure 11 shows that a combination of rest-frame UV (C IV $\lambda 1549$ /He II $\lambda 1640$) and rest-frame optical ([O III] $\lambda 5007$ /H β) emission line flux ratios can help to separate pure photoionization from shock dominated mechanisms. This diagram was derived assuming solar metallicity gas and is relatively insensitive to the effects of dust extinction as the ratios are determined from lines close in wavelength. Iwamuro (2003) conducted a rest-frame UV-optical emission line study of 15 radio galaxies with $2 < z < 2.6$. They found that there is a range in observed line-ratios suggesting that some objects are best explained with photoionization of low metallicity gas while others are consistent with the shock+precursor model. Carson et al. (2001) and Maxfield et al. (2002) found evidence for changing line ratios *within* sources, suggesting that the dominant ionization process are depends on the region of interest.

Based on previously published values of [O III]/H $\beta \approx 3.4$ and 2.8 for 4C 41.17 and B2 0902+34 re-

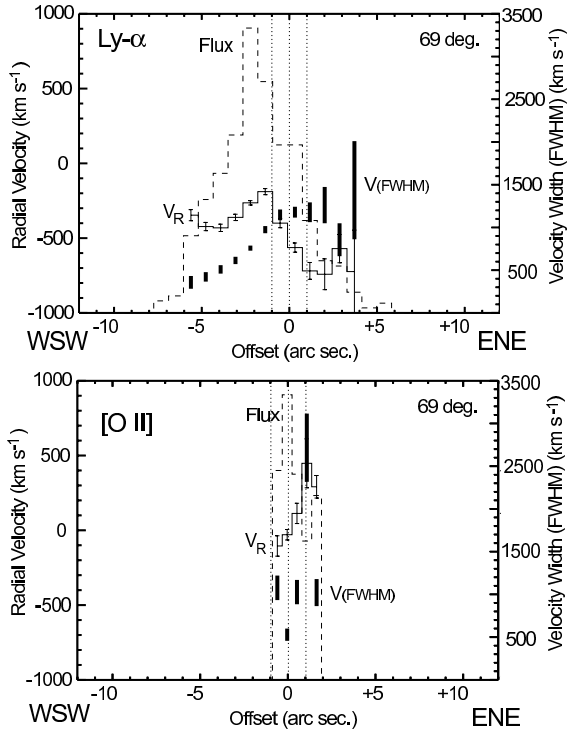


Fig. 10.— Similar to fig. 3 but for B2 0902+34. Ly α (top) and [O II] (bottom) both along PA=69 $^\circ$.

spectively (Eales & Rawlings 1993) it seemed that pure photoionization models could be ruled out. However the H β detections were marginal, and using the total integrated line fluxes for 4C 41.17 from the present study we derive ratios of [O III] λ 5007/H β \approx 9.6 for the central region and [O III] λ 5007/H β \approx 11.8 for the spatially integrated spectrum that are much higher and are consistent with both pure photoionization and shock+precursor models. The point derived for the spatially integrated spectrum of 4C 41.17 is also shown on fig. 11. This appears to show that the excitation of 4C 41.17 is similar to other radio galaxies. It cannot be due predominantly to stars, for which the [O III]/H β would be of order three and for which both C IV λ 1549 and He II would be very faint.

The extended regions of 4C 41.17 have a much lower excitation, however. As discussed in §3.1.1, for 4C 41.17, [O II] emission was detected as far as \approx 60 kpc from the nucleus. Figure 12 shows the velocity integrated relative intensities of Ly α and

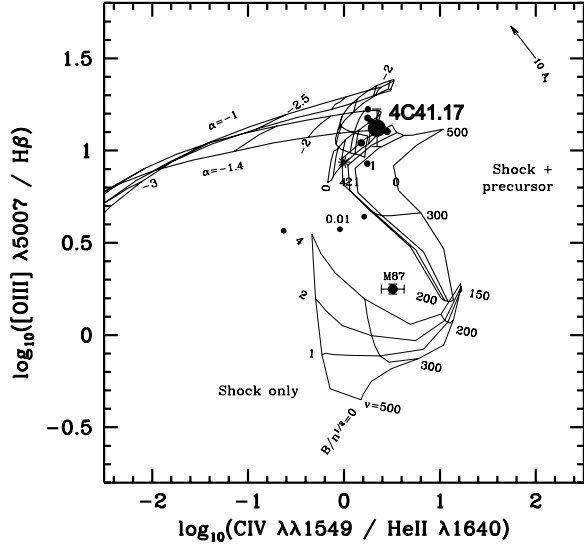


Fig. 11.— A UV-optical line diagnostic diagram adapted from Allen, Dopita & Tsvetanov (1998). The ratios [O III]/H β and C IV/He II are used to separate shock (lower grid), shock+precursor (right hand side) and photoionization (top left) models for solar metallicity gas. The shock models are marked according to the shock velocity and magnetic parameter, and the photoionization models according to the ionization parameter, U, and the power-law index of the photoionizing radiation field (α). The points represent nearby $z \approx 1$ Galaxies, and the accretion disk of M87 is explicitly identified. The large point with error bars is for the nucleus of 4C 41.17. This proves that the excitation of 4C 41.17 is similar to the other radio galaxies, and like them is shock-dominated.

[O II] as a function of distance from the nucleus for a red-shifted (+200 to +700 km s $^{-1}$) and a blue-shifted (−200 to −1000 km s $^{-1}$) velocity interval. The red-shifted [O II] flux closely follows that of the Ly α , while the blue-shifted [O II] shows a relative enhancement over the range 3–8'' W of the nucleus. In this region no evidence for [O III] is found (Fig. 2), whereas the [O III] emission in the nuclear region is much brighter than the [O II]. This shows that [O III]/[O II] ratio is much lower (\approx 1–2) in the outer regions than in the center (\approx 3–4) implying that a different mechanism is responsible for the extended [O II] emission. The

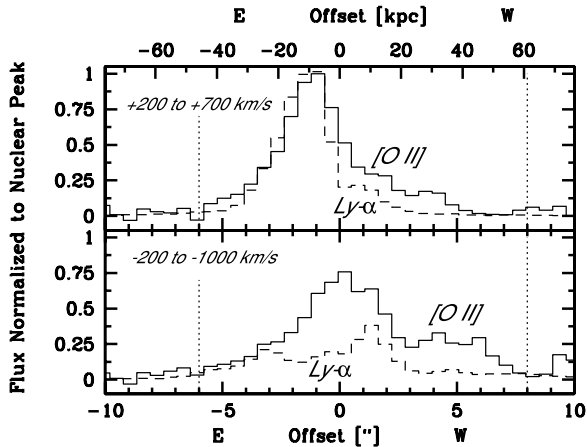


Fig. 12.— Top: Normalized surface brightness profiles of the [O II] (solid line) and $\text{Ly}\alpha$ (dashed line) emission along the inner radio axis and southwest filament of 4C 41.17. These are integrated in the velocity range $+200$ to $+700$ km s^{-1} and clearly show the spatially-extended [O II] emission. The spatial zero-point corresponds to the position of the radio core. Bottom: Similar to top panel but for the velocity range -200 to -1000 km s^{-1} . The [O II] emission is detected out to $\approx 8''$ (≈ 60 kpc) west of the nucleus, where it is blue-shifted by ≈ -600 km s^{-1} relative to the He II line. The projected distance of the south-west and north-east radio lobes along the slit direction are indicated (dotted lines). The $+200$ to -200 km s^{-1} range for [O II] is confused by near-infrared sky lines and is therefore not shown.

[O III]/[O II] ratio is known to be sensitive to the ionization parameter in the nebula. Because they have higher ionization parameters and also have central stars with higher effective temperatures for a given age, the low-metallicity H II regions are characterized by higher [O III]/[O II] ratios. Since this ratio falls to very low values in the outer parts of 4C 41.17 this proves that Population III stars with their very high effective temperatures cannot be responsible for the excitation of the outer regions. Excitation by shocks is a more likely ionizing source, since the emission is extended along the radio-axis and both the $\text{Ly}\alpha$ and [O II] are blue-shifted by ≈ 600 km s^{-1} . Furthermore, the peak in the [O II] emission on the W side of 4C 41.17 corresponds to the point at which the velocity dispersion drops steeply and boundary of the outer

radio lobe. This suggests that the [O II] is excited by shocks in an outward-propagating cocoon around the radio lobe. We note here that [O II] emission is particularly strong in shocks. This corroborates the suggestions by Dey et al. (1997) and Bicknell et al. (2000) that the $\text{Ly}\alpha$ emission, at least in this direction, is not due to scattering but that the nebula must be locally ionized by shocks related to radio source. Scharf et al. (2003) proposed that the escape of X-ray emission from the shocked region could be responsible for ionizing the extended halo beyond the the radio lobes.

From the jet shock spectrum, Bicknell et al. (2000) inferred that the metallicity of the star-forming cocoon around the radio jet was about the same as for the LMC; a half to a third of solar. For the nucleus itself, N V is often used as a tracer of the chemical abundance, because it is rather insensitive to shock ionization, density fluctuations, ionization parameter, and as a secondary nucleosynthesis element has a quadratic dependence on the metallicity (Villar-Martín et al. 1999; Groves, Dopita & Sutherland 2004a). This would imply that that would only be detected in highly chemically enriched sources, and not significant in the majority of HzRGs (Röttgering et al. 1997; De Breuck et al. 2000). Vernet et al. (2001) presented a metallicity sequence for HzRGs that is similar to the one for quasars (Hamann & Ferland 1993). 4C 41.17 was included in their study and a metallicity of $Z \approx 1.3 Z_{\odot}$ was inferred for the central region (aperture of $2'' \times 1''$ Dey et al. 1997).

Thus, the nuclear and jet cocoon spectra of 4C 41.17 argue for a fair degree of chemical enrichment, perhaps more in the nucleus than in the jet region. However, the halo region is by no means primordial in its abundances. Although we cannot directly infer the actual metallicity, we can say that the detection of strong [O II] emission out to ≈ 60 kpc from the nucleus demonstrates that the halo has been chemically enriched throughout its volume, at least in the illuminated regions.

A similar conclusion is also inferred for 4C 60.07. The very similar velocity morphologies and spatial extent of the $\text{Ly}\alpha$ and [O II] spectra at PA = 81° seen in figure 5 once again shows that the enriched gas is distributed throughout the $\text{Ly}\alpha$ halo. The strongly- C IV emitting shell in the nuclear vicinity shows that this galaxy too is excited primarily by the AGN rather than by star

formation. The expanding shell morphology of both Ly α and C IV further argues that 4C 60.07, like 4C 41.17, is excited mostly by shocks in the dense expanding cocoon of interstellar gas pushed by the relativistic jets from the nucleus.

4.2. Galaxy Mass estimates

The HzRGs are known to represent some of the most massive galaxies formed in the early universe. An estimate of their mass, by any means, is important to constrain the Λ -CDM models of galaxy formation, since the formation of such massive galaxies so early on might present something of an issue for the theory to resolve. We therefore provide these mass estimates in this section.

4.2.1. Luminosity based masses

van Breugel et al. (1999) estimated the mass of 4C 41.17 using the integrated rest-frame UV light. They found it to be a very massive galaxy with $L_{UV} \approx 17L^*$. Similarly, Graham et al. (1994) used near-IR imaging with the line-free K_S filter to estimate the mass of the galaxy directly. In a 4'' diameter aperture they found $K_S = 19.6 \pm 0.6$ mag. This converts in their cosmology to an absolute magnitude of 4C 41.17 to be $M_B = -23.0$, or about $20 L^*$.

A lower mass limit for the ionized gas in the halo can be obtained from photoionization modelling of the total Ly α flux, neglecting the effect of dust absorption, and assuming that the ISM is fully ionized. From this we derive an average thermal electron density in the halo of $n_{e,halo} = 0.1 f_v^{-\frac{1}{2}} \text{cm}^{-3}$ where f_v is the volume filling factor of the Ly α emitting gas. This yields a mass of gas of $M_{halo} \approx 6 \times 10^{12} f_v^{\frac{1}{2}} M_\odot$. For a volume filling factor $f_v \approx 1$ the inferred amount of gas is substantial and comparable to the broadband mass estimates of the host galaxy and that of fully formed, massive elliptical galaxies in the local Universe. However, the fact that the Ly α line appears to provide a good dynamical mass tracer, and is not grossly affected by self-absorption argues in favor of $f_v \ll 1$, and consequently, for a much lower total mass. The molecular component of 4C 41.17 has recently been traced by De Breuck et al. (2005), who have detected the CO(4-3) transition using the IRAM interferome-

ter. They find two massive CO clouds ($M_{dyn}^{rot} \approx 6 \times 10^{10} M_\odot$) which coincide with two different dark lanes located close to the nucleus in the deep Ly α image. This is similar to the CO content of the sub-millimetre galaxies, as measured by Greve et al. (2005) ($M_{CO} \approx 3 \times 10^{10} M_\odot$), suggesting once again that the HzRGs and the sub-millimeter galaxies are drawn from similar populations of galaxies, differing only in the activity of their AGN.

4.2.2. Dynamical mass estimates

van Ojik et al. (1997) and Villar-Martín et al. (2003) have presented mass estimates for the more quiescent parts of the emission line regions in their studies. There are two methods of estimating the dynamical masses. First, one can assume that the halos consist of gas that has settled in rotating disks. Secondly, the halos can be envisaged as consisting of virialized clumps, which have velocity dispersions that balance the gravitational forces.

In the case of rotating disks, the mass can be estimated by measuring the velocity shear across the halo and using: $M_{dyn}^{rot} = RV^2/G \sin^2 i$ with R the radius of the disk, V half the amplitude of the rotation curve, and i the inclination of the disk with respect to the plane of sky. Villar-Martín et al. (2003) found evidence for rotation in about $\approx 50\%$ of the objects they looked at and inferred masses of order $M_{dyn}^{rot} \times \sin^2 i \approx 0.3 - 3 \times 10^{12} M_\odot$.

Looking at our measured relative velocity distributions for 4C 41.17, we infer a velocity shear of $\approx 300 \text{ km s}^{-1}$ ($+100 \text{ km s}^{-1}$ to -200 km s^{-1}) at PA = 76°, over a distance of $R = 20''/2 = 77 \text{ kpc}$. From this we infer a dynamical mass of about $M_{dyn}^{rot} \times \sin^2 i \approx 4 \times 10^{11} M_\odot$. The velocity profiles at position angles PA = 19°, and 21° show no signs of a shear, consistent with their approximate alignment along the axis of rotation.

The observations for 4C 60.07 does not show an indication of being settled in a disk. Rather, it could be supported against gravitation by velocity dispersions of the cloudlets in the halo. For this scenario the dynamical mass is given by: $M_{dyn}^{vir} = 5RV_R^2/G$, with V_R the radial velocity dispersion of the clouds. Using this relation we derive dynamical masses for the outer regions of $M_{dyn}^{vir} = 5 - 10 \times 10^{11} M_\odot$. For the inner regions, where the signal-to-noise ratio is better we find

lower mass of $M_{\text{dyn}}^{\text{vir}} \approx 2 \times 10^{11} M_{\odot}$.

The Ly α emission profile of B2 0902+34 revealed by fig. 9 suggests a strong nuclear velocity shear. If this is interpreted as a rotation, then it would imply a rotational velocity of $\approx 550 \text{ km s}^{-1}$ over a distance of $3''$ or a rotation velocity of $\approx 275 \text{ km s}^{-1}$ at $R \approx 12 \text{ kpc}$. This implies a dynamical mass within this core region of $M_{\text{dyn}}^{\text{rot}} \times \sin^2 i \approx 2 \times 10^{11} M_{\odot}$. However, as discussed in section 3.1.7 this velocity gradient could equally well be due to the expansion of a shell of interstellar gas driven by the a directed bipolar outflow from the AGN with a velocity v_{exp} .

5. Outflows

Absorbing gas associated with lower velocity outflows has now been observed in several HzRGs, almost all of which show asymmetric Ly α profiles suggesting the presence of blue-shifted absorbing gas which appears to be spatially extended over the entire emission line region (see e.g., van Ojik et al. 1997; Dey 1999; Jarvis et al. 2003; Wilman et al. 2004). Spectroscopic evidence for outflows at high redshifts exists also for other, presumably less massive, galaxies (Pettini et al. 2001; Dawson et al 2002).

There is an ongoing debate whether massive ($> L_*$) galaxies or less massive ($< L_*$) galaxies enrich the ICM. Martin (1999) and Heckman et al. (2000) found that outflow speeds, v_{exp} , are largely independent of galaxy mass. This would imply that smaller galaxies are more efficient at ejecting enriched material to large radii. Specifically, Heckman (2002) claim that for massive galaxies the metals will not escape the deep potential wells. However, recent modelling suggests that the bulk of the metals in clusters are produced by L_* and brighter galaxies (e.g., Nagashima et al. 2004).

For all the three HzRGs we have observed, we found features that can be interpreted as symptomatic of outflows. The extended optical filament of 4C 60.07 is consistent with an outflow in the plane of sky. 4C 60.07 also shows crescent shaped arcs around the radio core and unobscured optical nucleus that are consistent with an expanding cocoon; see fig. 6. The blue-shifted carbon-rich component of B2 0902+34 seems to point towards an outflow of enriched material with an outflow velocity, v_{exp} of up to 1000 km s^{-1} .

The near-infrared [O II] spectroscopy (Figs. 2, 3, and 12) and the earlier optical Ly α spectroscopy of 4C 41.17 (Fig. 2; Dey et al. 1997), show that both emission lines exhibit large blue-shifted radial velocities $\approx 600 - 900 \text{ km s}^{-1}$ seen in projection along the radio axis. In particular, the gas is very disturbed along the south-west filament, with Ly α velocity widths ranging up to $\Delta v_F \approx 900 - 1600 \text{ km s}^{-1}$. Beyond the radio hotspot, the velocity and velocity widths decrease abruptly. The kinematics, its radial filamentary structure, and chemical enrichment of the gas all indicate a process of entrainment of material away from the central regions by the radio jet. In this scenario, the optical filament represents the shocked radiative cocoon of the radio source.

For a galaxy mass of $M_{\text{gal}} \sim 1 \times 10^{12} M_{\odot}$ within a radius of $R \sim 40 \text{ kpc}$, figures that seem to be typical for these HzRGs, the escape velocity $v_{\text{esc}} = (2GM/R_{\text{gal}})^{1/2}$ is of order $\sim 450 \text{ km s}^{-1}$. The velocity gradients found from the spectroscopic observations range a factor 1.5–2.5 larger than this, and implies that the ejection of the ISM originating from close to the nucleus of such galaxies is a viable scheme to both chemically enrich the inter-galactic medium and to terminate the epoch of star formation in these massive galaxies.

While it may still be true that purely starburst powered super galactic winds may not be sufficiently energetic for enriched nuclear material to escape from the galaxian potentials, the additional driving force produced by the energy content of the relativistic lobes produced by the central AGN seem quite able to blow matter out of the potential of the galaxy. This is direct evidence of the operation of the type of feedback process proposed by Silk & Rees (1998). In this, the growth of the super-massive central black hole is terminated by the ejection of the reservoir of interstellar gas, once the mass of the black hole exceeds a critical value. In their model, this critical value is determined by the relationship between the radiation pressure and the depth of the stellar potential, and it is able to provide a qualitative description of the Magorrian relationship (Magorrian et al. 1998), or the relationship between the mass of the central black hole and the velocity dispersion of the bulge (Magorrian et al. 1998; Ferrarese & Merritt 2000; Gebhardt 2000).

The observations presented here suggest that

this model needs to be modified somewhat. Rather than being driven by radiation pressure, the dynamical evidence is that they are driven by the PdV work done on the galactic medium by the relativistic jets, and that the ejection is occurring in the faster moving material in the shocked cocoon around the radio jet. Such a scheme is also suggested by the hydrodynamical simulations of Springel, Di Matteo, & Hernquist (2005). However, rather than being ejected isotropically in a disk-like galaxy, as in their model, in the HzRGs directional jets are being driven into a more spheroidal distribution of galactic interstellar gas. Given that 4C 41.17 has clear evidence of large amounts of shock-triggered star formation in this shocked cocoon, we can conclude that, in the HzRGs we are witnessing the fireworks that terminate the epoch of star formation in these massive galaxies – the last hurrah before these galaxies become massive “red and dead” Elliptical galaxies that we find today in the cores of the most massive clusters.

The multiple component, asymmetric, and twisted radio structure of 4C 41.17 suggests that during this phase, the central SMBH has experienced multiple periods of radio source activity and precession, (van Breugel et al. 1999; Steinbring, Crampton & Hutchings 2002). The precessing radio source will gradually evacuate the central region of the galaxy of its interstellar medium. The time scales for star formation and radio source activity in 4C 41.17 are very similar (Chambers, Miley & van Breugel 1990; Bicknell et al. 2000) and comparable to that for transporting the [O II] gas along the filament out to the vicinity of the south-west hotspot ($\approx 7 \times 10^7$ yrs at $\approx 900 \text{ km s}^{-1}$). It suggests an overall picture where the initial growth of the galaxy through merging, the feeding and growth of the central black hole, the growth of the stellar component, and finally triggering of SMBH the outflow, and its associated starburst activity are all closely coupled processes.

6. Conclusions

Extended Ly α halos are observed both in HzRGs and in the sub-millimetre galaxies. Indeed, these objects may be drawn from the same underlying population, with the distinction that

the HzRGs represent the radio-loud and active phase of the galaxian evolution. This seems supported by the observation that the largest radio-quiet Ly α halos have similar sizes and only slightly lower luminosities as the HzRGs but lack their large multi-component continuum structures.

Our long slit optical spectra of 4C 41.17, 4C 60.07 and B2 0902+34 have shown that their Ly α halos exhibit disturbed kinematics, with broad lines, large velocity shears, and, in some cases, expanding shells associated with the radio lobes. This clearly demonstrates that the relativistic jets are driving strong shocks into the galactic medium.

In 4C 41.17 the near-IR spectra reveal very extended [O II] and [O III] emission distributed along the radio source axis, as far as 60 kpc from the nucleus. This provides direct proof that the Ly α halos are both chemically enriched by star formation and ionized throughout the majority of their volume. The hypothesis that the Ly α is due to scattering off H I clouds is disproved. Likewise, the idea that the halo gas is primarily composed of chemically pristine “primordial” gas is also disproved. However, we cannot be certain that the gas in directions perpendicular to the radio axis contains a large primordial component, because the sensitivity of our spectroscopic observations is insufficient to detect Oxygen lines at the low surface brightness expected. To settle this point would require very deep near-IR spectroscopy of the halo gas *outside* the radio sources, well beyond the hotspots and orthogonal to the radio axes. This would be a very difficult observation to make.

Our observations of HzRGs also help cast observational light on the origin of the correlation found in galaxies between the stellar velocity dispersion and the black hole mass (Gebhardt 2000; Ferrarese & Merritt 2000). We find clear evidence of outflows of chemically enriched gas associated with the jets, and velocity dispersions in the expanding cocoons around the jets which probably exceed the escape velocity. In addition, B2 0902+34 shows Ly α absorption can be identified with a galaxy-wide outflow of material, similar to the galaxy-wide outflow identified by Wilman et al. (2005). This demonstrates that in the HzRGs the central black hole has grown sufficiently to be able to profoundly modify its sur-

rounding galactic medium, pushing it into outflow, and (in the case of 4C 41.17) triggering large quantities of star formation in the shocked galactic medium cocooning the radio lobes. Furthermore, the precession of the radio lobes seen in 4C 41.17 will ensure that eventually, all of the interstellar medium will be shocked and either be converted into stars, or else ejected from the galaxy.

These observations can be understood in terms of the general picture of Silk & Rees (1998) that feedback of the black hole on its host galaxy eventually limits the growth of the black hole. However unlike the Silk & Rees (1998) concept, the feedback process is not primarily radiation pressure but is the mechanical energy input delivered by the relativistic jets. Thus, in the HzRGs we may be observing the moment where galaxy collapse gives way to mass ejection, a newly born galaxy is revealed. We may speculate that this is the defining moment where the such galaxies enjoy one last violent burst of shock-induced star formation before beginning their evolution to become the “red and dead” massive Elliptical galaxies we see in our local universe.

We thank all staff at the W.M. Keck Observatory for their excellent support. The authors wish to recognize and acknowledge the very significant cultural role and reverence that the summit of Mauna Kea has always had within the indigenous Hawaiian community. We are most grateful to have the opportunity to conduct observations from this mountain. M.R. thanks Mario Livio and the Space Telescope Science Institute for generous hospitality. This work was performed under the auspices of the U.S. Department of Energy, National Nuclear Security Administration by the University of California, Lawrence Livermore National Laboratory under contract No. W-7405-Eng-48. WvB acknowledges support for radio galaxy studies at the Institute for Geophysics and Planetary Physics at Lawrence Livermore National Laboratory and at UC Merced, including the work reported here, with the Hubble, Spitzer and Chandra space telescopes via NASA grants HST GO-9779, GO-10127, SST GO-3482, SST GO-3329 and Chandra/CXO GO-06701011. M.D. acknowledges the support of the ANU and the Australian Research Council (ARC) for his ARC Australian Federation Fellowship, and also

under the ARC Discovery projects DP0208445 and DP0664434. This work was supported by the European Community Research and Training Network “The Physics of the Intergalactic Medium”. AD’s research is supported by NOAO, which is operated by the Association of Universities for Research in Astronomy (AURA), Inc. under a cooperative agreement with the National Science Foundation.

REFERENCES

- Aguirre, A. Hernquist, L., Schaye, J., Katz, N., Weinberg, D. H., & Gardner, J. 2001, *ApJ*, 561, 521
- Ahn, S. 2004, *ApJ*, 601, L25
- Allen, M. G., Dopita, M. A. & Tsvetanov, Z. I. 1998, *ApJ*, 493, 571
- Athreya, R. M., Kapahi, V. K., McCarthy, P. J., & van Breugel, W. 1998, *A&A*, 329, 809
- Benson, A. J.; Bower, R. G., Frenk, C. S., Lacey, C. G., Baugh, C. M. & Cole, S. 2003, *ApJ*, 599, 38
- Best, P. N., Röttgering, H. J. A. & Longair, M. S. 2000a, *MNRAS*, 311, 1
- Best, P. N., Röttgering, H. J. A. & Longair, M. S. 2000b, *MNRAS*, 311, 23
- Bicknell, G. V., Dopita, M. A., & ODea, C.P. 1997, *ApJ*, 485, 112.
- Bicknell, G. V., Sutherland, R. S., van Breugel, W. J. M., Dopita, M. A., Dey, A., & Miley, G. K. 2000, *ApJ*, 540, 678
- Briggs, F. H., Sorar, E. & Taramopoulos, A 1993, *ApJ*, 415, L99
- Carilli, C. L., Owen, F. N., Harris, D. E., 1994, *AJ*, 107, 480
- Carilli, C. L. 1995, *A&A*, 298, 77
- Carilli, C. L. Röttgering, H. J. A., van Ojik, R., Miley, G. K. & van Breugel, W. J. M. 1997, *ApJS*, 109, 1
- Carson, J. E., Larkin, J. E., McLean, I. S., Graham, J. R., Becklin, E. E., Figer, D. F., Gilbert, A. M., Levenson, N. A., Teplitz, H. I. & Wilcox, M. K. 2001, *ApJ*, 563, 63

- Chambers, K. C., Miley, G. K. & van Breugel, W. J. M. 1990, *ApJ*, 363, 21
- Chambers, K. C., Miley, G. K., van Breugel, W. J. M., Bremer, M. A. R., Huang, J.-S. & Trentham, N. A. 1996, *ApJS*, 106, 247
- Chapman, S. C., Lewis, G. F., Scott, D., Richards, E., Borys, C., Steidel, C. C., Adelberger, K. L. & Shapley, A. E. 2001, *ApJ*, 548, L17
- Charlot, S. & Fall, S. M. 1993, *ApJ*, 415, 580
- Cody, A. M. & Braun, R. 2003, *A&A*, 400, 871
- Dawson, S. Spinrad, H., Stern, D., Dey, A., van Breugel, W., de Vries, W. & Reul, M. 2002, *ApJ*, 570, 92
- De Breuck, C., Röttgering, H., Miley, G., van Breugel, W. & Best, P. 2000, *A&A*, 362, 519
- De Breuck, C., van Breugel, W., Stanford, S. A., Röttgering, H., Miley, G. & Stern, D. 2002, *AJ*, 123, 637
- De Breuck, C., Downes, D., Neri, R., van Breugel, W., Reuland, M., Omont, A. & Ivison, R. 2004, *A&A*, 430, L1
- di Serego Alighieri, S. and Cimatti, A. and Fosbury, R. A. E. & Hes, R. 1997, *A&A*, 328, 510
- Dey, A., van Breugel, W., Vacca, W. D. & Antonucci, R. 1997, *ApJ*, 490, 698
- Dey, A. 1999 in “The Most Distant Radio Galaxies”, eds. H. J. A. Röttgering, P. N. Best, and M. D. Lehnert, Royal Netherlands Academy of Arts and Sciences: Amsterdam, p19
- Dey, A., et al. 2005, *ApJ*, 629, 654
- Dopita, M. A., & Sutherland, R. S. 1996, *ApJS*, 102, 161
- Dopita, M. A., Koratkar, A. P., Allen, M. G., Tsvetanov, A., Ford, H. C., Bicknell, G. V., & Sutherland, R. S. 1997, *ApJ*, 490, 202.
- Dunlop, J. S., Hughes, D. H., Rawlings, S., Eales, S. A., & Ward, M. J., 1994, *Nature*, 370, 347
- Eales, S. A. & Rawlings, S. 1993, *ApJ*, 411, 67
- Egami, E., Armus, L., Neugebauer, G., Murphy, T. W., Soifer, B. T., Matthews, K. & Evans, A. S. 2003, *AJ*, 125, 1038
- Eisenhardt, P. & Dickinson, M. 1992, *ApJ*, 399, L47
- Ferrarese, L. & Merritt, D. 2000, *ApJ*, 539, L9, C. Ho, L. C. Kormendy, J. Lauer, T. R. Magorrian, J. Pinkney, J. Richstone, D. & Tremaine, S. 2000, *ApJ*, 539, L13
- Fosbury, R. A. E., Villar-Martín, M., Humphrey, A., Lombardi, M., Rosati, P., Stern, D., Hook, R. N., Holden, B. P., Stanford, S. A., Squires, G. K., Rauch, M. & Sargent, W. L. W. 2003, *ApJ*, 596, 797
- Gebhardt, K., Bender, R., Bower, G., Dressler, A., Faber, S. M., Filippenko, A. V., Green, R., Grillmair, C., Ho, L. C., Kormendy, J., Lauer, T. R., Magorrian, J., Pinkney, J., Richstone, D. & Tremaine, S. 2000, *ApJ*, 539, L13
- Graham, J. R., Matthews, K., Soifer, B. T., Nelson, J. E., Harrison, W., Jernigan, J. G., Lin, S., Neugebauer, G., Smith, G. & Ziomkowski, C. 1994, *ApJ*, 420, L5
- Greve, T. R., Bertoldi, F., Smail, I., Neri, R., Chapman, S. C., Blain, A. W, Ivison, R. J., Genzel, R., Omont, A., Cox, P., Tacconi, L. & Kneib, J.-P. 2005, *MNRAS*, 359, 1165
- Groves, B. A., Dopita, M. A. & Sutherland, R. S. 2004, *ApJS*, 153, 9
- Groves, B. A., Dopita, M. A. & Sutherland, R. S. 2004, *ApJS*, 153, 75
- Hamann, F. & Ferland, G. 1993, *ApJ*, 418, 11
- Heckman, T. M., Lehnert, M. D., Strickland, D. K & Armus, L. 2000, *ApJS*, 129, 493
- Heckman, T. M. 2002 in “Extragalactic Gas at Low Redshift”, eds. J. S. Mulchaey & J. Stocke, ASP Conference Proceedings, ASP:San Francisco, 254, 292
- Inskip, K. J., Best, P. N., Rawlings, S., Longair, M. S., Cotter, G., Röttgering, H. J. A., & Eales, S. 2002a, *MNRAS*, 337, 1381

- Inskip, K. J., Best, P. N., Röttgering, H. J. A., Rawlings, S., Cotter, G., & Longair, M. S. 2002, *MNRAS*, 337, 1407
- Iverson, R. J., Dunlop, J. S., Smail, I., Dey, A., Liu, M. C., & Graham, J. R. 2000, *ApJ*, 542, 27
- Iwamuro, F., Motohara, K., Maihara, T., Kimura, M., Eto, S., Shima, T., Mochida, D., Wada, S., Imai, S. & Aoki, K. 2003, *ApJ*, 598, 178
- Jarvis, M. J., Wilman, R. J., Röttgering, H. J. A. & Binette, L. 2003, *MNRAS*, 338, 263
- Kallman, T. R. & McCray, R. 1982, *ApJS*, 50, 263
- Kauffmann, G. & Haehnelt, M. 2000, 311, 576
- Kennicutt, R. C. 1998, *ARA&A*, 36, 189
- Lilly, S. J 1988, *ApJ*, 333, 161
- Loeb, A. 1993, *ApJ*, 403, 542
- Magorrian, J., Tremaine, S., Richstone, D., Bender, R., Bower, G., Dressler, A., Faber, S. M., Gebhardt, K., Green, R., Grillmair, C., Kormendy, J. & Lauer, T. 1998. *AJ*, 115, 2285
- Maier, C., Meisenheimer, K., & Hippelein, H. 1004, *A&A*, 418, 475
- Martin, C. L. 1999, *ApJ*, 513, 997
- Martin-Mirones, J. M., Martinez-Gonzalez, E., Gonzalez-Serrano, J. I. & Sanz, J. L. 1995, *ApJ*, 440, 191
- Massey, P., Strobel, K., Barnes, J. V. & Anderson, E. 1988, *ApJ*, 328, 315
- Maxfield, L., Spinrad, H., Stern, D., Dey, A. & Dickinson, M. 2002, *AJ*, 123, 2321
- McCarthy, P. J. 1993, *ARA&A*, 31, 639
- McLean, I. S., Becklin, E. E., Bendiksen, O., Brims, G., Canfield, J., Figer, D. F., Graham, J. R., Hare, J., Lacayanga, F., Larkin, J. E., Larson, S. B., Levenson, N., Magnone, N., Teplitz, H. & Wong, W. 1998, *Proc. SPIE*, 3354, 566
- Nagashima, M. Lacey, C. G. Baugh, C. M. Frenk, C. S. Cole, S. 2005, *MNRAS*, 363, 31
- Neufeld, D. A. 1990, *ApJ*, 350, 216
- Oke, J. B., Cohen, J. G., Carr, M., Cromer, J., Dingizian, A., Harris, F. H., Labrecque, S., Lucinio, R., Schaal, W., Epps, H. & Miller, J. 1995, *PASP*, 107, 375
- Overzier, R. A., Röttgering, H. J. A., Kurk, J. D. & De Breuck, C. 2001, *A&A*, 367, L5
- Pagel, B. E. J., Edmunds, M. G., Blackwell, D. E., Chun, M. S. & Smith, G. 1979, *MNRAS*, 189, 95
- Panagia, N., Stiavelli, M., Ferguson, H. & Stockman, H. S. 2003, *Rev. Mex. Ast. y Ap.*, 17, 230
- Papadopoulos, P. P., Röttgering, H. J. A., van der Werf, P. P., Guilloteau, S., Omont, A. & van Breugel, W. J. M. 2000, *ApJ*, 528, 626
- Pentericci, L., Van Reeve, W., Carilli, C. L., Röttgering, H. J. A. & Miley, G. K. 2000, *A&AS*, 145, 121
- Pettini, M., Shapley, A. E., Steidel, C. C., Cuby, J., Dickinson, M., Moorwood, A. F. M., Adelberger, K. L. & Giavalisco, M. 2001, *ApJ*, 554, 981
- Pettini, M. & Pagel, B. E. J. 2004, *MNRAS*, 348, 59
- Rauch, M., Sargent, W. L. W. & Barlow, T. A. 2001, *ApJ*, 554, 823
- Reuland, M., van Breugel, W., Röttgering, H., de Vries, W., Stanford, S. A., Dey, A., Lacy, M., Bland-Hawthorn, J., Dopita, M. & Miley, G. 2003, *ApJ*, 592, 755
- Röttgering, H. J. A., van Ojik, R., Miley, G. K., Chambers, K. C., van Breugel, W. J. M., & de Koff, S. 1997, *A&A*, 326, 505
- Scharf, C., Smail, I., Iverson, R., Bower, R., van Breugel, W. & Reuland, M. 2003, *ApJ*, 596, 105
- Shapley, A. E., Erb, D. K., Pettini, M., Steidel, C. C. & Adelberger, K. L. 2004, *ApJ*, 612, 108
- Sheinis, A. I. Miller, J. S. Bolte, M. Sutin, B. M. 2000, *Proc. SPIE*, 4008, 522
- Silk, J. Rees, M. J. 1998, *A&A*, 331, L1

- Springel, V., Di Matteo, T., & Hernquist, L. 2005, MNRAS, 361, 776
- Steinbring, E., Crampton, D. & Hutchings, J. B. 2002, ApJ, 569, 611
- Stevens, J. A. Ivison, R. J. Dunlop, J. S. Smail, I. R. Percival, W. J. Hughes, D. H. Röttgering, H. J. A. van Breugel, W. J. M. & Reuland, M. 2003, Nature, 425, 264
- Tody, D. 1993, “Astronomical Data Analysis Software and Systems II”, eds. R. J. Hanisch, R. J. V. Brissenden, and J. Barnes, A.S.P. Conference Ser. 52, 173
- Uson, J. M. Bagri, D. S. Cornwell, T. J 1991, Phys. Rev. Lett., 67, 3328
- van Breugel, W., Stanford, A., Dey, A., Miley, G., Stern, D., Spinrad, H., Graham, J., McCarthy, P. 1999, “The Most Distant Radio Galaxies”, eds. H. J. A. Rttgering, P. N. Best, and M. D. Lehnert., Royal Netherlands Academy of Arts and Sciences:Amsterdam, p49
- van Ojik, R., Röttgering, H. J. A., Carilli, C. L., Miley, G. K., Bremer, M. N. & Macchetto, F. 1996, A&A, 313, 25
- van Ojik, R., Röttgering, H. J. A., Miley, G. K. & Hunstead, R. W. 1997, A&A, 317, 358
- Vernet, J., Fosbury, R. A. E., Villar-Martín, M., Cohen, M. H., Cimatti, A., di Serego Alighieri, S. & Goodrich, R. W. 2001, A&A, 366, 7
- Villar-Martín, M., Fosbury, R. A. E., Binette, L., Tadhunter, C. N. & Rocca-Volmerange, B. 1999, A&A, 351, 47
- Villar-Martín, M., Vernet, J., di Serego Alighieri, S., Fosbury, R., Humphrey, A. & Pentericci, L. 2003, MNRAS, 346, 273
- Wilman, R. J., Jarvis, M. J., Röttgering, H. J. A & Binette, L. 2004, MNRAS, 351, 1109
- Wilman, R. J., Gerssen, J., Bower, R. G., Morris, S. L., Bacon, R., de Zeeuw, P. T., & Davies, R. L 2005, Nature, 436, 227

TABLE 1
RADIO GALAXY SAMPLE

Source	RA (J2000)	DEC (J2000)	z
B2 0902+34	09 05 30.11	34 07 55.9	3.389
4C 60.07	05 12 55.17	60 30 51.1	3.789
4C 41.17	06 50 52.14	41 30 30.7	3.798

NOTE.—Positions of the radio core (Carilli, Owen & Harris 1994; Carilli et al. 1997; Carilli 1995) and the systemic redshifts based on the He II line are adopted as the frame of reference in this paper.

TABLE 2
SUMMARY OF OBSERVATIONS AND INSTRUMENTAL SETUPS SORTED BY POSITION ANGLE (P.A.)

Object	Date	Instrument	Setup	Seeing (")	Slit (")	Resln. (Å)	λ Coverage (Å)	P.A. (deg)	Obs.Time (s)
B2 0902+34	16/01/02	LRIS	LS 600/5000	0.9	1.5	4	5150–7650	68.7	2×1800
	07/01/02	NIRSPEC	Low Disp. N5	0.9	0.76	14	14600–17400	68.5	6×900
4C 60.07	15/01/02	LRIS	LS 600/7500	0.7	1.5	4	5450–7600	81.0	2×1800
	25/02/01	ESI	Low Disp.	0.8	1.0	13 ^a	4000–9600	135.2	3.5×1800
4C 41.17	07/01/02	NIRSPEC	Low Disp. N6	0.9	0.76	14	15600–19800	81.4	6×900
	24/02/01	LRIS	LS 600/7500	0.7	1.5	6	5200–6100	19.4	3×1800
	23/02/01	LRIS	MOS 300/5000	0.6	1.0	4	4300–6600	21.6	4×1800
	10/12/96	LRISp	LS 400/8500	0.9	1.0	8	5500–9280	76.5	28×1200 ^b
	15/01/02	LRIS	MOS 400/8500	0.7	1.0	6	5300–8000	81.0	3×1800
	03/02/97	LRIS	LS 600/5000	0.9	1.0	5	4320–6850	170.8	3×1800
	07/01/02	NIRSPEC	Low Disp. N6	0.9	0.76	14	15600–19800	42.7	3×900
07/01/02	NIRSPEC	Low Disp. N6	0.9	0.76	14	15600–19800	70.2	5×900	
07/01/02	NIRSPEC	Low Disp. N7	0.9	0.76	14	20300–25000	42.7	2×900	
07/01/02	NIRSPEC	Low Disp. N7	0.9	0.76	14	20300–25000	67.8	4×900	

^aNear the redshifted Ly α line at $\lambda = 5825$ Å; the resolution varies roughly linearly from 3 Å at 3900 Å to 40 Å at 11000 Å.

^bSpectropolarimetric observations, a detailed analysis of which was presented in Dey et al. (1997).

TABLE 3
SUMMARY OF EMISSION-LINE MEASUREMENTS

Object	Line	λ_{rest} (Å)	λ_{obs} (Å)	z	FWHM (Å)	FWHM (km s^{-1})	Continuum Flux ($10^{-17} \text{ erg s}^{-1} \text{ cm}^{-2}$)	Line Flux (cm^{-2})	EW_{obs} (Å)
B2 0902+34 (core)	Ly α	1215.7	5334.69 \pm 0.09	3.3883 \pm 0.0001	21.9 \pm 0.2	1233 \pm 13	18.3 \pm 0.5	7890 \pm 95	431 \pm 12
	C IV(doublet)	1549.0	6795.00 \pm 0.62	3.3867 \pm 0.0004	22.7 \pm 1.5	1003 \pm 65	16.3 \pm 0.4	1770 \pm 70	109 \pm 5
	He II	1640.5	7199.37 \pm 0.37	3.3886 \pm 0.0002	17.2 \pm 0.9	715 \pm 37	11.8 \pm 0.4	1502 \pm 60	127 \pm 7
B2 0902+34 (total)	Ly α	1215.7	5336.26 \pm 0.23	3.3896 \pm 0.0002	21.4 \pm 0.4	1203 \pm 24	27.4 \pm 3.8	25640 \pm 600	937 \pm 133
	C IV(doublet)	1549.0	6799.58 \pm 0.72	3.3897 \pm 0.0005	10.4 \pm 1.7	460 \pm 75	21.6 \pm 2.9	2590 \pm 420	120 \pm 25
	He II	1640.5							
4C 60.07 (core)	Ly α	1215.7	5826.52 \pm 0.07	3.7928 \pm 0.0001	47.1 \pm 0.2	2424 \pm 12	\leq 0.01	41.1 \pm 0.2	\geq 5000
	C IV	1548.2	7415.7 \pm 0.37	3.7899 \pm 0.0004	81.4	6 \times 900			
	C IV	1550.8	7428.1 \pm 0.37	3.7899 \pm 0.0004					
	He II	1640.5	7855.7 \pm 1.07	3.7887 \pm 0.0007	73.9 \pm 2.7	2820 \pm 105	\leq 0.01	9.5 \pm 0.3	\geq 790
	C III]	1908.7	9140.7 \pm 1.70	3.7889 \pm 0.0007					
4C 60.07 (total)	Ly α	1215.7	5824.59 \pm 0.18	3.7913 \pm 0.0002	44.9 \pm 0.5	2310 \pm 25	\leq 0.01	56.1 \pm 0.7	\geq 4000
	C IV(doublet)	1549.0	7420.75 \pm 1.34	3.7907 \pm 0.0009	36.5 \pm 3.3	1475 \pm 130	\leq 0.01	5.0 \pm 0.3	\geq 600
	He II	1640.5	7848.50 \pm 4.41	3.7843 \pm 0.0027	84	3220 \pm 4400	\leq 0.02	4.0 \pm 1.6	\geq 230
	C III]	1908.7	9141.88 \pm 1.82	3.7896 \pm 0.0010	59.9 \pm 4.7	1960 \pm 155	\leq 0.01	0.2 \pm 0.8	\geq 14
	Ly α	1215.7	5818.07 \pm 0.29	3.7859 \pm 0.0002	20.0 \pm 0.7	1030 \pm 36	\leq 0.01	6.2 \pm 0.2	\geq 6600
4C 60.07 (filament)	[O II]	3727.0	6973.30 \pm 0.33	0.8710 \pm 0.0001	30.0 \pm 0.8	1290 \pm 34	\leq 0.06	9.0 \pm 0.1	140
4C 60.07 (nearby galaxy)	[O II]	3727.0	7046.98 \pm 4.25	0.8908 \pm 0.0011	51.7 \pm ?	2200 \pm 450	\leq 0.02	3.7 \pm 0.2	\geq 180
4C 41.17 (core)	Ly α	1215.7	5834.5 \pm 0.1	3.8002 \pm 0.0001		613/1373 \pm 13/45		146 \pm 5.5	
	C IV	1548.2	7428.9 \pm 0.2	3.7984 \pm 0.0001		541 \pm 14		7.5 \pm 0.2	
	C IV	1550.8	7441.2 \pm 0.2	3.7984 \pm 0.0001		541 \pm 14		5.7 \pm 0.2	
	He II	1640.5	7870.7 \pm 0.4	3.7979 \pm 0.0002		553 \pm 28		5.5 \pm 0.3	
	C III]	1908.7	9152.5 \pm 0.6	3.7951 \pm 0.0003		511/1120 \pm 151/135		9.1 \pm 0.2	
	[O II]	3727.0	17890.36 \pm 0.54	3.8002 \pm 0.0001	42.4 \pm 1.1	711 \pm 18	57.8 \pm 7.1		
	H β	4861.0	23351.72 \pm 3.27	3.8039 \pm 0.0007	33.0 \pm 8.1	424 \pm 104	0.19 \pm 0.04	17.2 \pm 4.9	92.7 \pm 32.9
	[O III]	4959	23816.29 \pm 1.20	3.8026 \pm 0.0002	36.1 \pm 3.0	454 \pm 38	0.18 \pm 0.04	59.8 \pm 5.2	337.8 \pm 81.2
	[O III]	5006.9	24046.74 \pm 0.42	3.8027 \pm 0.0001	37.9 \pm 1.1	472 \pm 13	0.18 \pm 0.04	222.8 \pm 5.4	1260 \pm 295
	H β	4861	23355.84 \pm 8.35	3.8047 \pm 0.0017	55	700 \pm 270	0.47 \pm 0.12	52.5 \pm 21.5	112 \pm 54
4C 41.17(total)	[O III]	4959	23810.62 \pm 3.03	3.8015 \pm 0.0006	50.8 \pm 7.8	640 \pm 98	0.50 \pm 0.14	129.4 \pm 20.5	259 \pm 85
	[O III]	5006.9	24041.56 \pm 1.13	3.8017 \pm 0.0002	58.4 \pm 3.0	728 \pm 37	0.47 \pm 0.16	484.7 \pm 22.6	1031 \pm 351

NOTE.—Where two values are given, line is split.